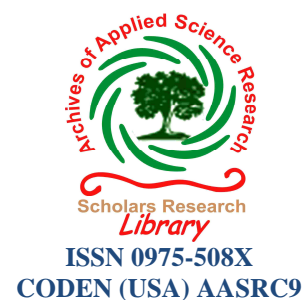




Scholars Research Library

Archives of Applied Science Research, 2012, 4 (5):2244-2255  
(<http://scholarsresearchlibrary.com/archive.html>)



## Thermostability, Alloying ability, Growth Habits and Micromechanical Parameters of Aluminium Rich Al-Cd-Sn Composite

Parshotam Lal and B. L. Sharma

ISCAS Institute of Solid State and Materials Science, Jammu University Campus, Jammu-180 006, India

### ABSTRACT

The current work is conducted with an aim to accrue comprehensive understanding of the growth habits of an analog of aluminium rich composites from the melt to explore the superiority of micromechanical parameters in the domain of anisotropic alignment of microstructural parameters. Homogeneous chemical composition and liquidus temperature of the fabricated composite Al-Cd-Sn are ascertained by DSC technique, and alloying ability of the constituent phases is established by X-ray diffraction study. The scanning electron microscope is used in the analysis of surface structures of the composite phases at variable anisotropic growth rates. Computed Vickers micromechanical parameters of the composite at variable anisotropic growth velocity under constant applied load of  $50 \times 10^{-2} \text{ N}$  in the experimental load range from  $10 \times 10^{-2} \text{ N}$  to  $100 \times 10^{-2} \text{ N}$  for a definite time interval 10s, are found to follow an identical form of the Weibull probability distribution curve. Naturally occurring constants with the micromechanical parameters are extensively studied for physical understanding of the plastic deformation.

**Keywords:** property combination, moderate growth, aligned lamellae, fracture toughness, plastic deformation.

### INTRODUCTION

With an extensive knowledge of various types of composites as well as understanding of the dependence of their physical properties, particularly the mechanical behavior on the lamellae alignment, relative amounts and properties of the constituent phases, it is possible to design the materials with property combinations that are better than those found in the metal alloys, ceramics and polymeric materials [1-5]. Modern technologies require materials with unusual combinations of properties that cannot be met by the conventional metal alloys, ceramics and polymeric materials. This is especially true for materials that are needed for aerospace, underwater, and transportation applications. For example, aircraft engineers are increasingly searching for structural materials that besides low densities, are strong, stiff, abrasion and impact resistant, and not easily corroded. This is a rather a terrific and formidable combination of characteristics particularly when these materials are fabricated by an anisotropic process [6-9]. Frequently, strong materials that are available, are relatively dense; also, increasing the strength or stiffness generally results in a decrease in impact strength. Material property combinations and ranges have been, and are yet being, extended by the development of composite materials. Generally speaking, a composite is considered to be any multiphase material that exhibits a significant proportion of the properties of the constituent phases of different space groups such that a better combination of properties is realized. In designing composite materials, scientists and engineers have ingeniously combined various metals, ceramics and polymers to produce a new generation of extraordinary materials [10-14]. Most composites have been created to improve combinations of mechanical characteristics such as stiffness, toughness, and ambient and high-temperature strength.

As reported earlier [15] a generation of new aluminium-lithium alloys have been developed recently for use by the aircraft and aerospace industries, however these materials are more costly in fabrication than conventional alloys because special processing technologies are required to control lithium's chemical reactivity. All lamella reinforced

aluminium-composites show a higher elastic modulus, a lower co-efficient of thermal expansion and higher wear resistance compared to conventional alloys. The machining behavior is more difficult compare to standard alloys but depends strongly on particle-size and system [16-20]. Their (aluminium-composites) elastic modulus varies from 90 to 220 GPa. To be consistent with the principle of better combinations, an analog of Al-Cd-Sn of aluminium rich composites is designed as modal product by following an efficient anisotropic growth in the domain of variable solidification rates from the melt. Because of the complex nature of the phenomena involved in an anisotropically controlled solidification from the melt, a considerable judgment is required to assess both theoretical and experimental results, since the composites that can be obtained by this process exhibit a large diversity of micromorphologies. Nevertheless, a physical understanding of the mechanical properties of products obtained by controlling the growth rates from the melt can readily be distinguished when examined in electron microscopes. A succinct implicitness in the present approach is the ability to put strong, stiff lamellae in the right place, in the right orientation with the right volume fraction, since the essence of composite materials technology is the concept to design materials with unique properties as acceptable analog for manufacturing the engineering products. Vickers micromechanical parameters at variable anisotropic growth velocity follow an identical form of the Weibull distribution curve demonstrating the strength-growth relationship. Thermal and X-ray diffraction studies of ternary composite Al-Cd-Sn phases ascertain thermal stability, melting and liquidus temperatures, enthalpies of fusion and mechanical combination of homogeneous phases.

## MATERIALS AND METHODS

### Experimental

The composite alloy Al-Cd-Sn was prepared in the pyrex tube by weighing a proper amount of purity 99.999% Al [Alfa Aesar, AR, mp 949 K,  $\Delta_f H = 10.80 \text{ kJmol}^{-1}$ ], 99.999% Cd [Alfa Aesar, AR, mp 597 K,  $\Delta_f H = 6.19 \text{ kJmol}^{-1}$ ] and Sn [Alfa Aesar, AR, mp 509 K,  $\Delta_f H = 7.30 \text{ kJmol}^{-1}$ ] shots with 40 wt% Al, 30 wt% Cd and 30 wt% Sn. The melting temperatures and enthalpies of fusion of the constituent metals, cited in the parentheses, were obtained by thermal analysis approaching very closely to their literature values. The ampoule tube was sealed under vacuum to avoid oxidation and infused in a furnace set a temperature  $\sim 900 \text{ K}$  for alloying Al, Cd and Sn metals to Al-Cd-Sn composite. Homogeneity of the composite was ensured by heat-chill process keeping the temperature of the heater (air oven)  $\sim 700 \text{ K}$  and that of the cooler (water bath)  $\sim 300 \text{ K}$ . The liquidus temperature of the composite alloy Al-Cd-Sn (457 K) was also ascertained by thermal analysis.

#### i) Anisotropic growth

The experimental composite alloy Al-Cd-Sn was subjected to oriented growth in the following experimental setup. An experimental sealed pyrex tube containing half-full melt of a freshly prepared composite was clamped to the centre of an empty graduated beaker (volume capacity  $\sim 1 \text{ dm}^3$ ) manipulated midmost in an air oven set at a temperature 30K higher than its liquidus temperature. The molten mass in the tube was nucleated by circulating silicone oil at 18 different intervals spanned in the time range 50-60 min from the oil reservoir perforated and plugged with a glass tube carrying valve to control the percolation at  $\sim 300 \text{ K}$ . The melt in the tube started nucleating when the rising level of the oil just touched the bottom of the tube. Many a sample of the composite was grown anisotropically at different but nearly consistent growth rates determined by circulating approximately the same volume of the oil for each selected interval. The anisotropic solidification process offers mechanically efficient lamellae structure of the composite called 'modal product' at the moderate growth mode ( $\sim 2.90 \times 10^{-7} \text{ m}^3 \text{ s}^{-1}$ ).

#### ii) Instantaneous solidification

Isotropic growth was performed by immersing an experimental pyrex tube containing the composite melt in an ice bath maintained at  $\sim 273 \text{ K}$ . The growth being instantaneous in nature, is presumed of zero order. Likewise, several samples of composite phases were solidified for the isotropic growth for observations.

#### iii) Microscopic studies

The specimen grown anisotropically and isotropically were polished at room temperature following a procedure similar to that adopted for analogous problem [11] To reveal the microstructure, a thin layer of the specimen etched in ferric chloride was mounted on stub with gold-coated holder and examined under a scanning electron microscope for microgrowth observation. Many samples of each specimen were viewed in this manner and the growth habits of the growing phases during solidification at different growth rates were accordingly photographed.

#### iv) Vickers test

Indentations were induced on selected points chosen diagonally on an anisotropically or instantaneously grown composite sample at room temperature ( $\sim 300 \text{ K}$ ), using a Vickers microhardness tester attached to an incident-light metallurgical research microscope in the applied load ranging from  $10 \times 10^{-2}$  to  $100 \times 10^{-2} \text{ N}$ . For each test, a very small diamond indenter having pyramidal geometry was forced into the surface of the specimen at room temperature

and the size of the indent was found growing with rising applied load. Vickers micromechanical parameter of composite alloy Al-Cd-Sn was computed by the following relation [5, 9]:

$$\text{Vickers hardness, } H_v = \frac{1.8544P}{d^2} \quad (1)$$

where P is the applied load in Newton force and d is an average diagonal length of the indentation mark in meter. The parameter P depends on both the size of specimen being tested and the nature of the test, while d varies with the size of the crack. Experimental evidences are such that they emblematically acknowledge the unique mechanical property of the modal product.

#### v) X-ray diffraction studies

The X-ray diffraction patterns exhibited by the experimental composite phases were recorded with Diffraction System-XPRT=PRO using  $\text{CuK}\alpha$  radiation of wavelength 1.5408 Å at room temperature. The powder X-ray was recorded in a 2θ range of 5° to 90° with the step size of 0.05 and step time of 1s.

### RESULTS AND DISCUSSION

The DSC curve resulted in by the thermal analysis of the composite alloy Al-Cd-Sn is presented in Fig. 1 explicitly exhibiting its thermal stability, homogeneity and liquidus temperature. Micromorphological images of the composite phases oriented at different growth rates are pictorially displayed in Fig.2. The mutual tendency of the lamellae alignment accomplishing microstructural parameters of the composite in the anisotropic growth process presents their relationship with mechanical aptitude. Micromechanical parameter is found most probable at the moderate anisotropic growth ( $\sim 2.90 \times 10^{-7} \text{m}^3 \text{s}^{-1}$ ) which a unique finding in the present work searched out in the experimental growth observations by setting the flow- interval of silicone oil at  $5.0 \times 10^{-4} \text{m}^3$  for 28 min, this particular process of solidification strengthens the composite lamellae to exhibit optimum mechanical ability in the present investigation.

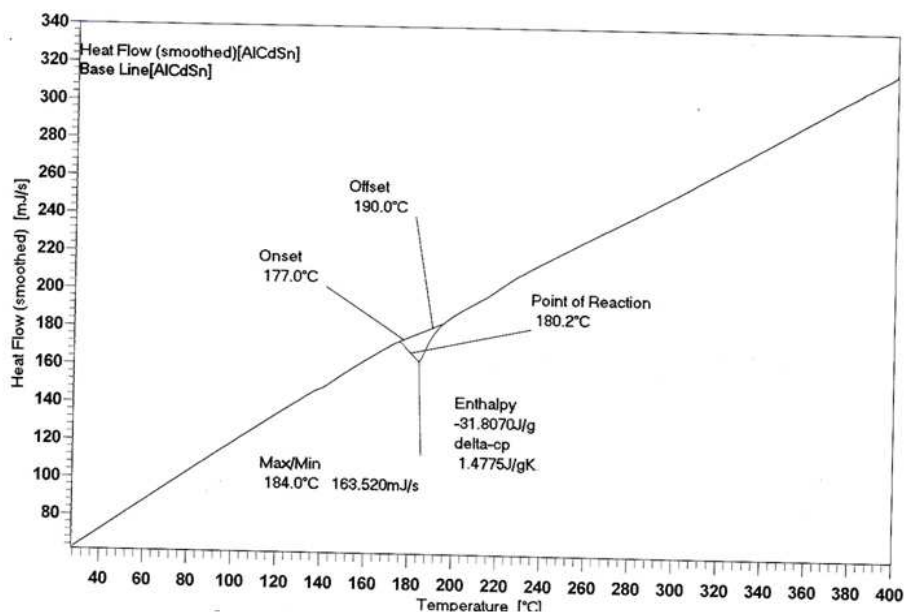
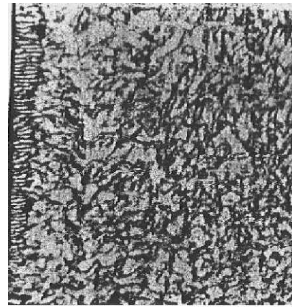


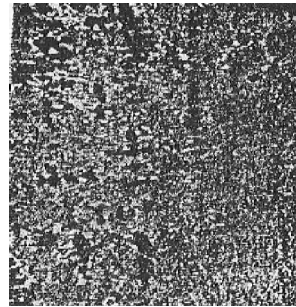
Fig. 1: DSC curve of composite alloy Al-Cd-Sn

The indentation impression inflicted composite specimens solidified at variable anisotropic growth rates (18 intervals) selected in the present work with a constant load of  $50 \times 10^{-2} \text{N}$  for indentation time 10s were subsequently subjected to micromechanical tests under Vickers microhardness tester and the variation of computed micromechanical parameters thereof in the experimental growth range strictly follow the Weibull probability distribution curve Fig.3. Verily, the curve is an important deduction of the linear; nonlinear and linear variant mechanical-growth inflexions in the slow; moderate and fast growth regions respectively. The microstructural parameters seem to follow the Weibull distribution in both the slow and fast growth regions resulting in their random habits. On the contrary, the microstructural parameters in the moderate growth region tender to follow the

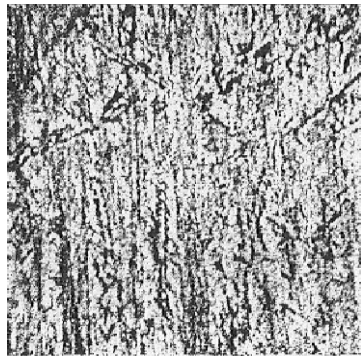
Gauss distribution by arranging themselves in preferred alignment. The moderate region of the curve paves the formation of modal microstructure of the composite appropriately called the modal product.



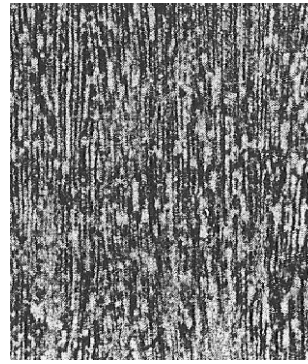
(a)



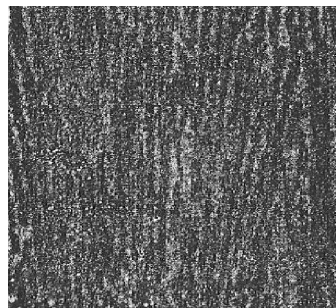
(b)



(c)



(d)



(e)

**Fig. 2. Micromorphological of the composite Al-Cd-Sn (1500x)**

(a) Distorted microstructure (isotropic) of composite phase lamellae in ice bath at  $\sim 273$  K (fast growth region); (b) evolution of composite phase lamellae in growth direction from bottom to top in the slow growth region,  $1.50 \times 10^{-7} \text{ m}^3 \text{ s}^{-1}$ ; (c) and (d) composite phase lamellae in the growth direction from bottom to top in the moderate growth region, at  $2.40 \times 10^{-7}$  and  $3.60 \times 10^{-7} \text{ m}^3 \text{ s}^{-1}$ , and (e) lamellar composite phase, growth direction from bottom to top at moderate anisotropic growth  $2.90 \times 10^{-7} \text{ m}^3 \text{ s}^{-1}$

The micromorphological images of the indented specimen of the modal product with different loads, and also with a constant load  $50 \times 10^{-2}$  N at variable induction time are present in figs.4 (a-e). Succinctly, the following inferences are drawn from the combination of figs. 3 and 4 which strongly confirm the plastic deformation of the modal product.

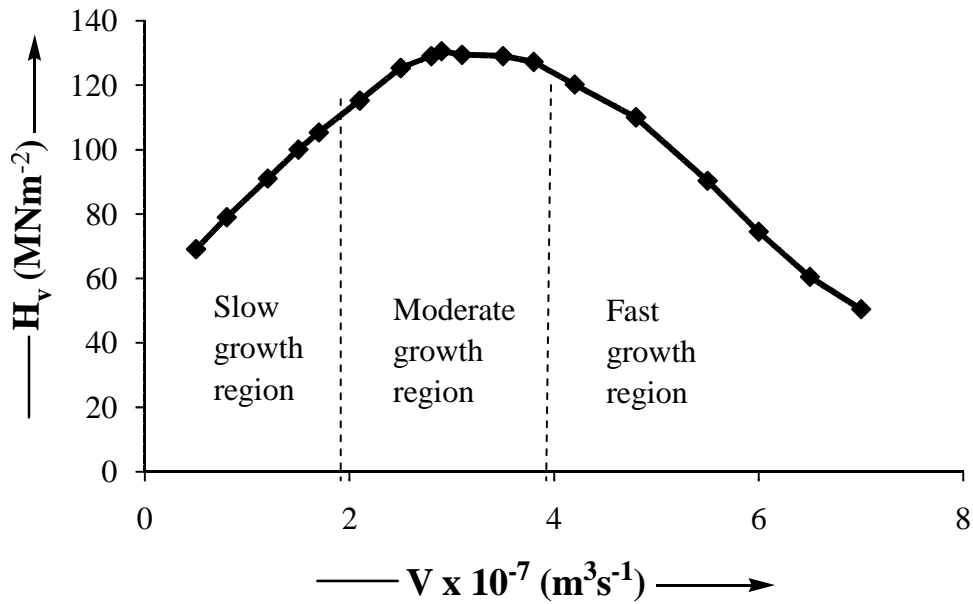
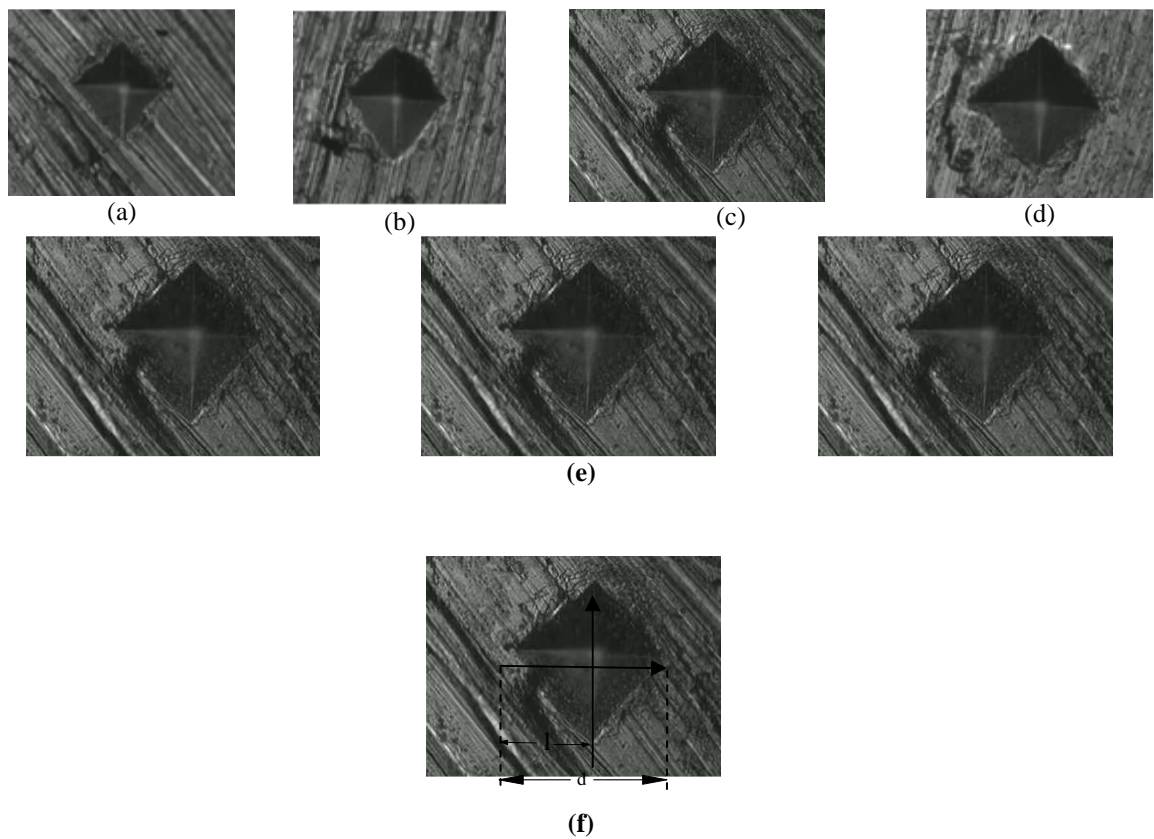
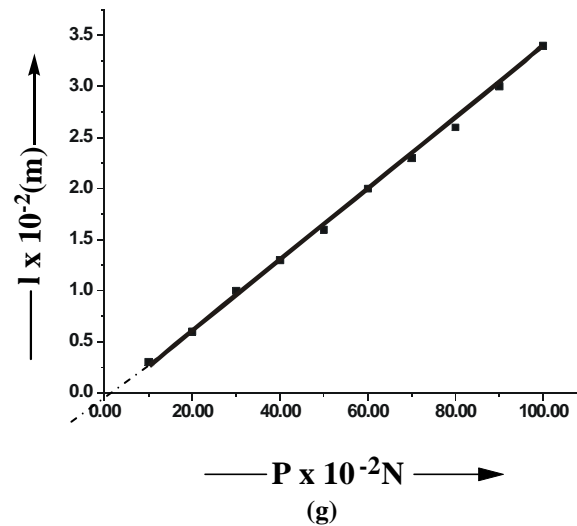


Fig.3. Variation of microhardness of the composite alloy Al-Cd-Sn over the entire range of experimental growth velocity elocity

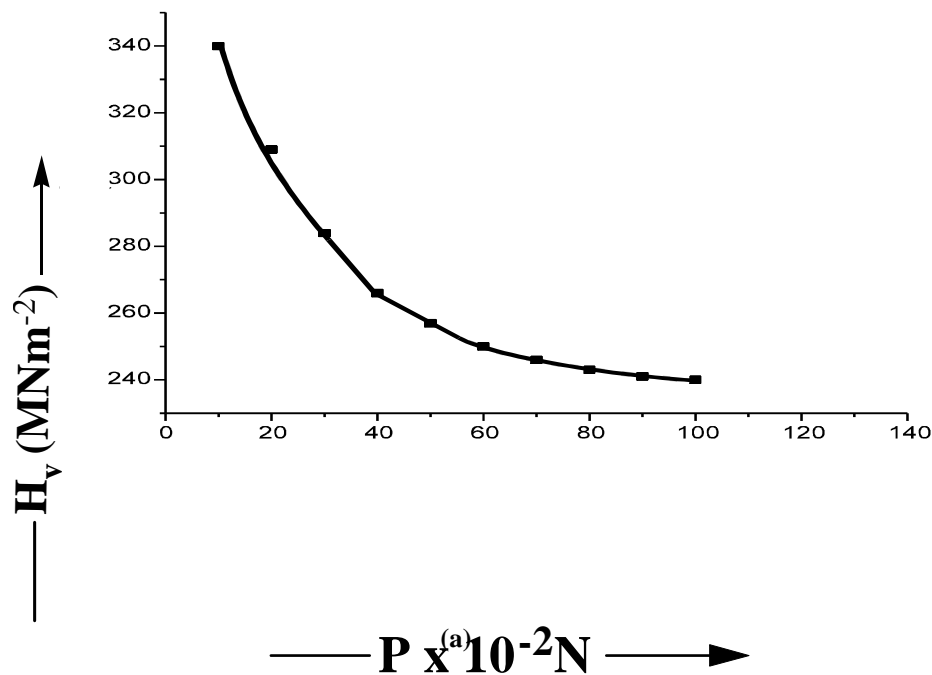




**Fig. 4: Photomicrographs showing indentation impressions on modal composite alloy Al-Cd-Sn under variable conditions (625 x)**

(a) Size of indentation with a load of  $10 \times 10^2 \text{ N}$ ; (b) size of the indentation with a load of  $20 \times 10^2 \text{ N}$ ; (c) size of indentation with a load of  $50 \times 10^2 \text{ N}$ ; (d) size of the indentation with a load of  $100 \times 10^2 \text{ N}$ ; (e) invariable size of indentation for a constant applied load of  $50 \times 10^2 \text{ N}$  at 50, 100 and 150s; (f) measurement of crack length and (g) plot showing variation of crack length with applied load.

Figure 2 indicates the ability of the moderate anisotropic growth ( $\sim 2.90 \times 10^{-7} \text{ m}^3 \text{ s}^{-1}$ ) in producing and putting strong, stiff, lamellae of the composite in the right place, in the right orientation with right volume fraction resulting in thereupon the formation of its modal product Fig.2e. Evidentially, the modal product at the aforementioned anisotropic growth attain lamellar structure comprising of strong lamella-matrix bond in comparison to slow and fast growth process producing fragile matrix because of the aggressive, non attaching and crossing develop habits of the lamellae responsible for its distorted structures Fig 2 ( a-d). The authenticity of the develop micromorphological structure to be the final (modal) product is evidentially verified by determination of its micromechanical parameter relatively upholding the optimum value which obviously be the theoretical strength an experimental extraction that can be visualized in Fig. 3.



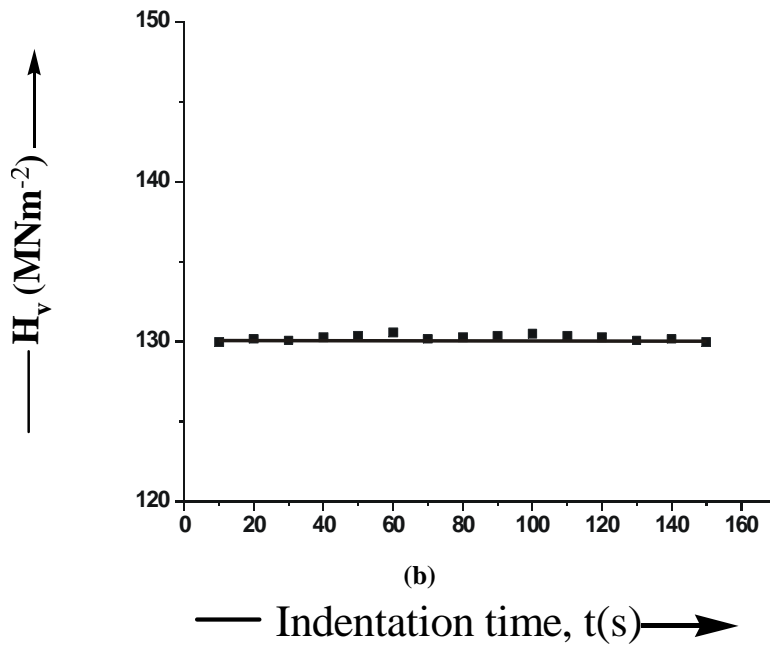
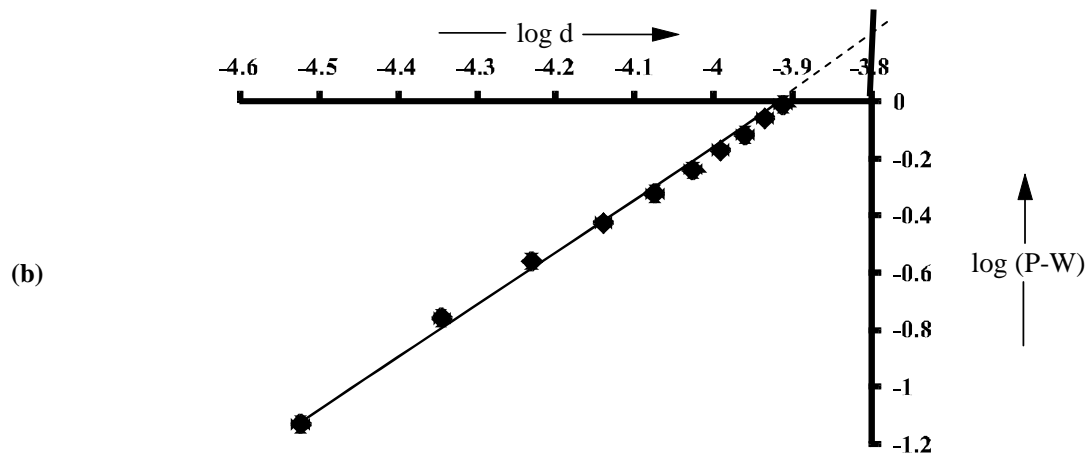
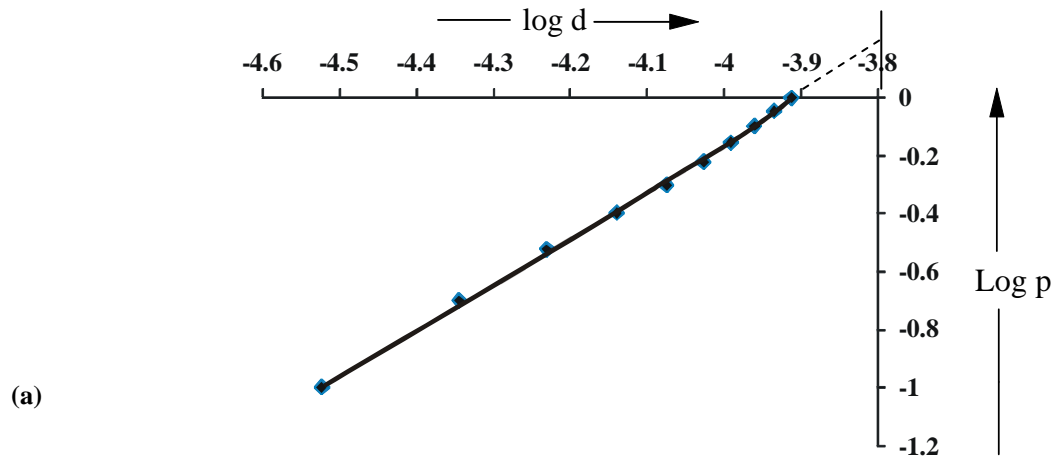
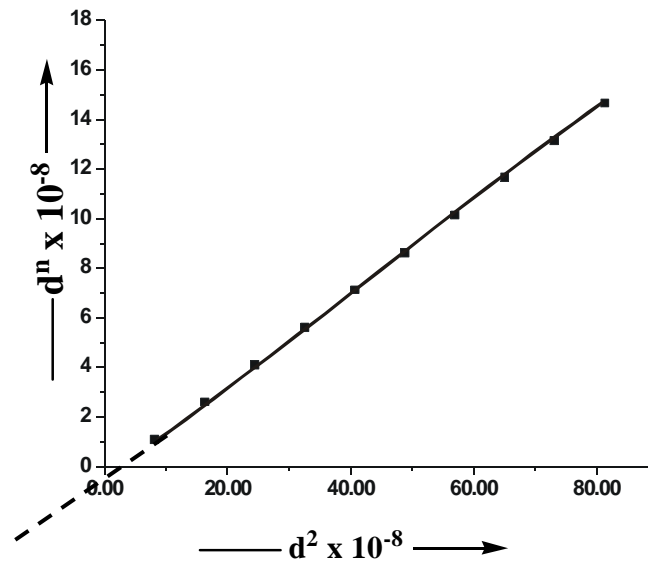


Fig.5: Variation of microhardness for the modal composite alloy Al-Cd-Sn.

(a) Nonlinear with variable applied load at constant indentation time,  $t$  (10s) and (b) linear with variable indentation time for constant load  $P$  ( $50 \times 10^{-2}N$ ).





(c)  
**Fig.6: Depiction of relations between the variables:**

(a)  $\log P$  and  $\log d$ ; (b)  $\log (P-W)$  and  $\log d$  and (c)  $d^n$  and  $d^2$

**Table 1**

S.No	Applied Load $P \times 10^{-2} \text{N}$	Crack Length $(l \times 10^{-2} \text{m})$	Fracture toughness $K_{Ic} (\text{Nm}^{-3/2})$	Vickers Hardness $H_v (\text{MNm}^{-2})$	Brittleness Bi ( $10^6 \text{m}^{-1/2}$ )	Yield strength $\sigma_y$ $(\text{MNm}^{-2})$
1	10	0.3	86.94	205.00	2.35	68.33
2	20	0.6	61.47	180.00	2.92	60.00
3	30	1.0	42.85	160.00	3.73	53.33
4	40	1.3	38.55	140.00	3.63	46.66
5	50	1.6	35.29	130.00	3.68	43.33
6	60	2.0	30.30	125.00	4.12	41.66
7	70	2.3	28.66	123.70	4.31	41.23
8	80	2.6	27.26	123.00	4.51	41.00
9	90	3.0	24.74	122.84	4.96	40.94
10	100	3.4	22.78	122.98	5.39	40.99

The concept of occurrence of plastic deformation during modal product testing is further strengthened by theoretical and experimental evidence discussed in the succeeding analyses.

**Theoretical extraction**

For plastic deformation the Kick’s law speaks that micromechanical parameters,  $H_v$  remain constant irrespective of the magnitude of a applied load,  $P$  [21 ] Numerically,  $P = k_1 d^n$  (2)

where Meyer's index  $n = 2$ , accounts for constant  $H_v$ , and  $k_1$  is a constant.

The literature also indicates the decrease and increase of  $H_v$  with rising applied load for materials culminating  $n < 2$  and  $n > 2$  respectively. Since the hardness whether micro or macro level is the resistance ability of a material to localized permanent deformation, the relationship between the Newtonian resultant pressure  $W$  in Newton of the material itself and area of indentation,  $A$  in  $\text{m}^2$  is the  $W/A$  ratio. The Hays and Kendall Hypothesis for plastic deformation, states that the actual load applied to the specimen is  $P-W$  in lieu of  $P$ . This resultant process of a material represents the minimum applied load to cause indentation as the applied load less than  $W$  by definition, will not, result in plastic deformation [22-23]. This Hypothesis thereupon taking the specimen resistance pressure  $W$  into account, modifies Eq. (2) of Kick’s law into the following valid form;

$$(P-W) = k_2 d^2 \tag{3}$$

where  $k_2$  and  $W$  are constants. Further, the evaluation of  $W$  follows the procedure necessarily involving subtraction of Eq. (2) from Eq. (3) which results in:

$$d^2 = \left(\frac{k_2}{k_1}\right) d^2 + \frac{W}{k_1} \quad (4)$$

The relation yields the parameters  $W$  from the theoretical and experimental known values of other parameters defined earlier.

### Experimental Extraction

The experimental facts obtained are consistent with the theoretical aspects available in the literature for the plastic deformation. The nonlinear relationship between experimental observed,  $H_v$  and the applied load  $P$  (Fig. 5a) implies that Vickers hardness ( $H_v$ ) decreases with an increasing applied load until about  $70 \times 10^2$  N and thereafter, a saturation stage of  $H_v$  starts occurring which is full at  $80 \times 10^2$  N. Qualitative explanation of this variation can be suggested that the penetration depth of the indenter with variable applied load is an appropriate consideration to reveal effective rupture of the specimen layers. Comprehensively, the indenter penetrates only surface layers of specimen with small applied load, the effect is more pronounced at these loads. Nevertheless, as the penetration depth increases with the applied varying loads the inner layers' damage of specimen appears to be more effective shattering the ability of hardness to the extent that  $H_v$  must become independent of further applied load which actually happened in the experimental range of applied load particular at and beyond  $80 \times 10^2$  N in the current work. The behavior is consistent with the microhardness increase at loads during early stages of plastic deformation. A plot between  $\log P$  and  $\log d$  (Fig. 6a) is linear and according to Eq(2) yields  $n$  and  $k_1$  for any set of discrete data, the index  $n$  being determined by the slope, while the  $k_1$  by the intercept, defined as the particular load  $P$  that exists at  $d = 10^{-3}$  m. In present investigation,  $n$  and  $k_1$  respectively obtained by Fig. 6a are 1.4302 and 1.2302 MPa.

Furthermore, plot of  $\log (P-W)$  versus  $\log d$  of Eq. (3) suggesting the logarithmic index  $n=2$ , drawn in Fig. 6b yields the value of the logarithmic index,  $n < 2$ , ( $n=1.4302$ ), thus confirming the validity of the Newtonian resistant pressure theory for the composite specimen, as mentioned earlier,  $W$  allows the limiting case to prevail whereat hardness becomes independent of load.

Analogically, a plot for  $d^n$  ( $n=1.4302$ ) versus  $d^2$  (Fig. 6c) yields the slope  $k_2/k_1$  (0.1854) and  $W/k_1$  ( $21.92 \times 10^{-8}$  m<sup>2</sup>) which  $k_2$  and  $W$  are separately calculated from the known value of  $k_1$  determined by the plot Fig. 6a, to their respective values 6.632 MPa and  $2.6977 \times 10^2$  N furnishing a compilation of key data on microhardness. Toughness virtually measures the ability of a material absorbing energy up to fracture. Moreover, fracture is a property indicative of material's resistance to fracture when a crack is present. The crack developed on the composite specimen determines the fracture toughness  $K_c$ , which specifies the extent to which fracture stress is applied on a uniform loading by the relation:

$$K_c = \frac{P}{\beta l^{3/2}} \quad (5)$$

where  $l$  is the radius of a semicircular radial crack or the crack length measured from the centre of the indentation mark to the crack tip.  $\beta$  is a numerical constant that depends on indenter geometry. For a Vickers indenter  $\beta = 7$ . However, Eq. (5) yields satisfactory values of the fracture toughness only if  $l \geq 3$  or  $l/a < 3$ , respectively for median or radial crack system (Fig. 4f) where 'a' exactly equals half diagonal length, i.e.,  $a = d/2$ . Table 1 records the values of crack length,  $l$  and fracture toughness,  $K_c$  for the composite specimen at different applied loads. Figure 4(g) is a plot between applied load,  $P$  and crack length,  $l$  indicating the linear dependence of the crack length on the increasing applied load. Brittleness is an important property, usually termed as the brittleness index  $B_i$ , which can be determined from  $K_c$  values obeying the relationship [24]:

$$B_i = \frac{H_v}{K_c} \quad (6)$$

the values of  $B_i$  obtained from Eq. (6) for the composite specimen at variable microhardness-fracture toughness ratio, are presented in Table 1. The yield strength of the composite computed from the hardness data at variable applied load using the valid equation [9] for  $n < 2$ :

$$\sigma_y = \frac{1}{3} H_v \quad (7)$$

the values estimated for the composite in the experimental load ranging from  $10 \times 10^2$  to  $100 \times 10^2$  N for an indentation interval of 10 s are also incorporated in Table 1. All the aforesaid parameters are well computable, and their computation collectively, accomplishes inferential analyses that authenticable the plastic deformation of the

modal composite Al-Cd-Sn in the present investigation. These observations are strongly supported by Fig.5b indicating the microhardness of the composite to be independent of variation in the indentation time for a constant load of  $50 \times 10^{-2}$ N at room temperature and revealing the occurrence of plastic deformation which remains unaffected with variable indentation time. Table 2 summarized the X-ray data, whereas Fig.7 shows X-ray patterns of the composite Al-Cd-Sn.

Table 2: XRD data of composite alloy Al-Cd-Sn

Pos. [°2TH.]	d-spacing [Å]	Intensity[Å]	Intensity [%]	Planes hkl
30.545	2.9243	301.0	59.7	Sn(200)
31.916	2.8017	363.0	70.5	Cd(002)
34.646	2.5870	118.0	22.8	Cd(100)
37.059	2.4239	33.6	6.5	Cd(101)
38.313	2.3474	515.0	100.0	Al(111)
43.818	2.0644	122.0	23.7	Sn(220)
44.830	2.0201	265.0	51.4	Al(200)
47.759	1.9028	82.7	16.1	Cd(102)
55.294	1.6600	64.4	12.5	Sn(301)
61.029	1.5170	92.0	17.9	Cd(103)
62.197	1.4913	70.9	13.8	Cd(112)
62.459	1.4857	109.0	21.1	Sn(112)
63.744	1.4588	40.1	7.8	Sn(400)
64.543	1.4426	69.4	13.5	Sn(321)
65.041	1.4328	52.9	10.3	Al(220)
66.461	1.4055	25.9	5.0	Cd(004)
71.587	1.3117	75.5	14.7	Cd(112)
72.375	1.3046	45.5	8.8	Sn(420)
73.148	1.2927	47.2	9.2	Sn(411)
75.751	1.2546	41.1	8.0	Cd(201)
78.189	1.2215	52.1	10.1	Al(311)
79.472	1.2050	78.4	15.2	Sn(312)
82.106	1.1728	28.3	5.5	Cd(202)
82.382	1.1696	31.9	6.2	Al(222)
89.394	1.0951	41.4	8.0	Al(421)
30.545	2.9243	301.0	59.7	Sn(200)
31.916	2.8017	363.0	70.5	Cd(002)
34.646	2.5870	118.0	22.8	Cd(100)
37.059	2.4239	33.6	6.5	Cd(101)
38.313	2.3474	515.0	100.0	Al(111)
43.818	2.0644	122.0	23.7	Sn(220)
44.830	2.0201	265.0	51.4	Al(200)

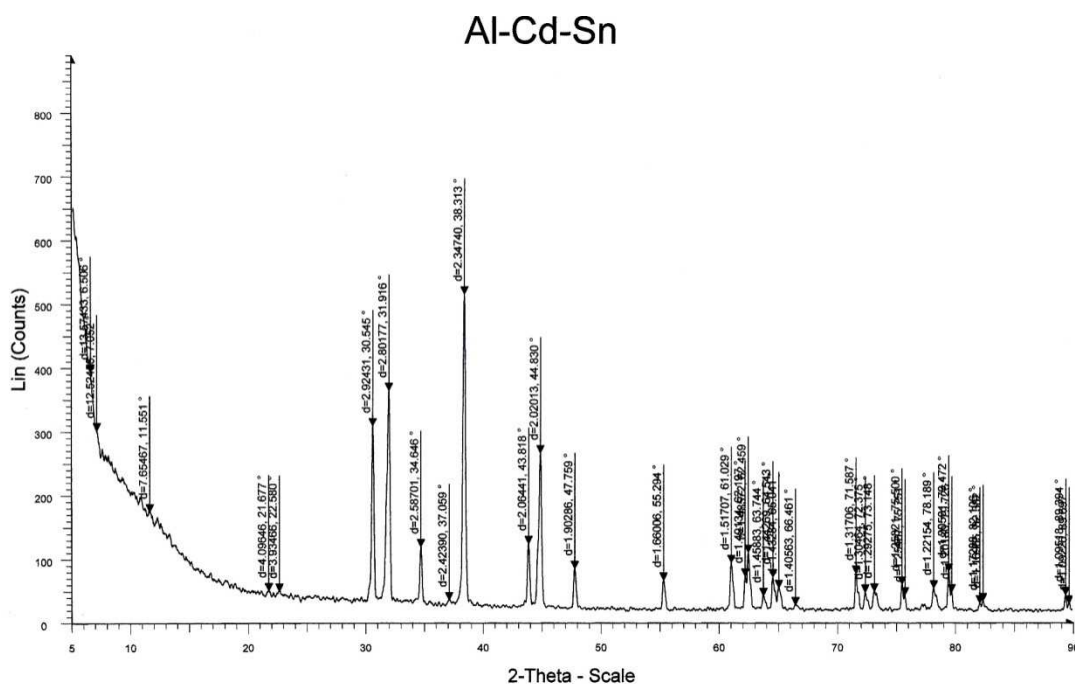


Fig.7: XRD patterns of composite alloy Al-Cd-Sn

The analysis of X-ray diffraction patterns (Fig. 7) and extracted diffraction data thereby (Table 2) for the composite Al-Cd-Sn, reveals the sharp lines of face centred cubic phases of aluminium, hexagonal phases of cadmium and body centered tetragonal phases of tin. This implies that the X-ray diffraction pattern analysis implicitly, inculcates the existence of the composite as a mechanical mixture of constituent metals simulating weak interactions because of their atomic electronegative character, since no unique diffraction line is exhibited by the composite. The physical significance of the observations extracted from the X-ray analysis, is that the composite is not a solidus solution but a terminal solidus solution.

### CONCLUSION

Microstructural parameters in the slow and fast growth tend their obedience to the Weibull distribution. However, they start showing deviation in the moderate growth region by alignment which is full at moderate growth velocity ( $\sim 2.90 \times 10^{-7} \text{m}^3 \text{s}^{-1}$ ) because of their obedience to the Gauss distribution. The micromechanical parameter (microhardness) of composite in the slow growth regions is similar, an experimental evidence, to that of the fast growth region, but its uniqueness in the moderate region, particularly at the moderate anisotropic growth is a significant aspect of the current work. The microhardness of the composite is found independent of the indentation time but does follow the non-linear dependence with variable applied load. The initiation of the crack on the composite specimen with the required minimum load affirms the applicability of the Newtonian theory of its resistance pressure. The generation of the radial cracks by an indenter loaded with pressure ranging from  $10 \times 10^{-2}$ - $100 \times 10^{-2} \text{N}$  facilitates the procedure to estimate the values of fracture toughness, brittleness index and yield strength of the composite specimen. The inferential significance of the mechanical parameters extracts the concept that the properties of the composite are superior and possibly unique to the properties of the pure constituent metals particularly, when its modal product is achieved by moderate anisotropic growth. Thermal analysis reveals thermal stability and liquidus temperatures of the composite. Moreover, the physical understanding of the X-ray studies defines the composite to be a terminal solidus solution of the constituent metals stimulating weak interactions at their atomic levels.

### REFERENCES

- [1] WD Callister Jr., Materials Science and Engineering: An Introduction, John Wiley & Sons, Inc (2004).
- [2] D Hull, TW Clyne, An Introduction to Composite Materials: III<sup>rd</sup> edition (Cambridge University Press, 2008).
- [3] W D Callister, G David Rethwisch, Composites: Polymer-Matrix Composites. Fundamentals of Materials Science and Engineering, 3<sup>rd</sup> ed. Hoboken, NJ: Wiley (2008).
- [4] D Hull, TW Clyne, An Introduction to Composite Materials: 2<sup>nd</sup> edition (1996).
- [5] BL Sharma, Parshotam Lal, Growth Reinforcing Composite Materials from Liquidus Phases: Mechanical and Microstructural Parameters Relationship Essentially Evincing the Predominance of an Akin Mass Composite over the Domain of Composition, Metal, Ceramic and Polymeric Composite for Various uses, John Cuppoletti (Ed.) ISBN: 1978-953-307-353-8 In Tech (2011).
- [6] D Hull, An Introduction to Composite Materials, Cambridge University Press, Cambridge (1985).
- [7] W Albers, in: H Muller (Ed.), Preparative Methods of Solid State Chemistry, Academic Press, New York (1972).
- [8] BL Sharma, Parshotam Lal, Monika Sharma, Arun Kumar Sharma. *J. Therm Anal. Calorim* DOI 10-1007/S/0973-011-1673-8 (2011).
- [9] Arun K Sharma, Parshotam Lal, B K Gandotra, R Kant, B L Sharma, *Arch. Appl. Sci. Res.* 2012, 4, 111-127.
- [10] BL Sharma, S Tandon, S Gupta. *Cryst. Res. Technol.* 2009, 44, 258-268.
- [11] DE Ovesienko, GA Alfinster, in: T Arizumi (Ed.), Crystal Growth, Properties and Application, Springer-Verlag, Berlin 1980, 2.
- [12] CR Tottle, An Encyclopedia of Metallurgy and Materials, LXVI, Macdonald and Evans Ltd., Great Britain (1984).
- [13] R Caram, WR Wilcox, *J. Mater. Process, Manuf. Sci.* 1992, 1, 56.
- [14] DR Lide, CRC Handbook of Chemistry and Physics, A Ready-Reference Book of Chemical and Physical Data 90<sup>th</sup> ed. CRC Press, London (2009).
- [15] Parshotam Lal, Shallu Abrol, BL Sharma, *Arch. Appl. Sci. Res.* 2012, 5.
- [16] G R, VD Bhandankav, BM, Suryvanshi, *Arch. Appl. Sci. Res.*, (2012), 1-4
- [17] V Renganaki, D Syamala, R Sathyamoorthy, *Arch. Appl. Sci. Res.*, (2012) 1453-1461
- [18] T Thaila and S Kumarraman, *Arch. Appl. Sci. Res.*, (2012)1494-1501
- [19] R Josephine Usha, J Arul Martinmani, P Sagayaraj, V Joseph, *Arch. Appl. Sci. Res.*, (2012)1545-1552
- [20] R Caram, M Banan, WR Wilcox, *J. Cryst. Growth* 1991, 114, 249.
- [21] KJ Pratap, VH Babu, *Bull. Mater. Sci.* 1980, 2, 43.
- [22] C Hays, EG Kendall, *Metallograpy*, 1973, 6, 275.
- [23] BR Lawn, ER Fuller, *J. Mater. Sci.* 1975, 9, 2016.

[24] K Nihara, R Morena, DPH Hasselman, *J.Mater. Sci. Lett.* **1982**, **1**, 13.